GNSS Multi-Frequency Multi-System Highly Robust Differential Positioning Based on an Autonomous Fault Detection and Exclusion Method

XIAO LIANG [ID], ZHIGANG HUANG, HONGLEI QIN, AND YICHEN LIU

School of Electronic and Information Engineering, Beihang University, Beijing 100191, China

Corresponding author: Honglei Qin (qhlmmm@sina.com)

ABSTRACT GNSS multi-frequency multi-system carrier phase differential positioning has become the main technology used in high-precision positioning. Until recently, the fault detection and exclusion (FDE) methods for multi-frequency multi-system carrier phase differential positioning mostly focus on procession of errors in the carrier phase domain, which cannot exclude all the faults causing a faulted baseline resolution, e.g., a fault that occurs in resolution process. Besides, the multi-fault of multi-frequency in the carrier phase domain cannot be identified due to the multi-frequency carrier phase observation errors' high correlation. We present a method of autonomous FDE based on multi-frequency multi-system carrier phase differential positioning. It focuses on the procession of errors in the position domain, and detects and excludes the faults in different frequency baseline resolutions caused not only by measurement fault as traditional method, but also the resolution fault, which can enhance the robustness and accuracy of the differential positioning system. The experimental results show that the method can effectively detect and exclude the failure of different frequency baseline resolutions and then the accurate multi-frequency multi-system positioning results can subsequently be effectively fused. The proposed method improves the accuracy and robustness of the differential positioning system.

INDEX TERMS Carrier phase differential positioning, fault detection and exclusion, GNSS, multi-frequency multi-system.

I. INTRODUCTION

Satellite navigation systems have been widely used in various fields, and the overall trend regarding such systems is to provide high-precision services for real-time applications. Although single-frequency receivers have low hardware costs, satellite navigation positioning results of a single frequency receiver are less reliable and less robust because of their small number of observations, making it difficult to use them effectively in a variety of complex environments. In addition, a single satellite navigation system cannot have guaranteed integrity, robustness, continuity and availability; in particular, in certain high-precision positioning applications, as well cannot meet the needs of indicators or ensure that the system continues to work reliably. To improve the reliability and robustness of the satellite navigation and positioning system, further improvement of the accuracy of positioning systems, multi-frequency bands or additional constellations are required for joint positioning, which can fully utilize multi-frequency multi-system signal to strengthen the robustness and availability of

the system. At present, the Global Positioning System (GPS) includes 31 available satellites and three civil frequencies of L1/L2/L5; the GLONASS system has 23 available satellites and three civil frequencies of L1/L2/L3; and the BeiDou Navigation System (BDS) includes 23 available satellites and three civil frequencies of B1/B2/B3. The continuous improvement of these satellite navigation systems is important for obtaining a high-precision and high-robustness multi-frequency multi-system positioning system.

Research institutions have conducted in-depth studies with the aim of fully utilizing the redundancy of multi-frequency multi-system. As early as 1982, Hatch proposed a classic linear combination with a dual-frequency carrier phase and pseudorange, eliminating the effects of the first-order ionosphere, troposphere, receiver clock error, and satellite clock error, which simplified the data processing model and improved the processing efficiency [1]. Ordonez conducted the first differential positioning experiments combining GPS and GLONASS, and showed that multi-system differential positioning had a positive effect on these sys-

X. Liang *et al.*: GNSS Multi-Frequency Multi-System Highly Robust Differential Positioning Based on an Autonomous FDE Method

IEEE*Access*

tems [2]. He et al. obtained the positioning results of a BeiDou/GPS dual-frequency single epoch for the first time. The results of the 8 km short baseline static positioning using the UB240 BD2/GPS dual-mode receivers were based on a single-epoch geometric correlation of the double difference model [3]. The results indicated that the dual-frequency positioning outperformed the single-frequency positioning and that multi-frequency multi-system positioning outperformed multi-frequency single-system positioning. The positioning accuracy of the dual-frequency dual-system was 5 cm. Chu et al. achieved a tri-frequency dual-system joint solution by combining GPS and Galileo triple-frequency observations. Under the simulation conditions, a baseline resolution accuracy of 4 mm was achieved under 134 km-long baseline conditions [4].

The multi-frequency multi-system guarantees the high robustness of the positioning system. But faults will lead to various resolutions of GNSS multi-frequency multi-system, which is so called multi-value problem. Thus, the multi-value problem must be solved by detecting and excluding the fault results and realizes high positioning precision by fusing accurate results. At present, there are mainly two types of methods for fault detection and exclusion for carrier phase differential positioning systems in the carrier phase domain. The detection–identification–adaptation (DIA) method is used to perform the quality control and fault exclusion [5]. However, when using DIA in carrier phase domain for single satellite data diagnose, carrier phase errors cannot be easily identified due to the high correlation between multi-frequency carrier phase observation errors [6]. Besides, it is difficult for DIA to specify the appropriate alternative hypotheses for a particular application. And another type of method based on the combination of observations or Kalman filtering processing is proposed for specific error, e.g. cycle slips, multipath [7]–[9]. These methods are inapplicable to the multi-frequency multi-system positioning system, where the multi-failures from different sources occur simultaneously for a high possibility. Moreover, existed FDE are processed in the carrier phase domain, some small outliers in carrier phase measurements may not be excluded, as these could affect the baseline resolution. Even if there are no outliers in the carrier phase measurements, the resolution processing of positioning results may also result in faults. For example, in the integer ambiguity resolutions, the determined optimal solution may not the right solution, which will influence the positioning result. In the position domain, different frequency positioning results can be compared to avoid faults of integer ambiguity resolutions at some frequencies. The capability gap is why the reported method in the position domain is important.

The method proposed adopts high-precision carrier phase differential positioning to resolve baseline resolutions of various frequencies of different systems respectively and uses the consistency of the baseline vector to detect faults and fuse accurate solutions. If there is no fault in a frequency, the sum of the squared errors (SSE) of carrier baseline observation residual vector follows the chi-square distribution; otherwise, it will not follow the chi-square distribution. Thus, a chi-square test is used for fault detection, which differs from traditional ones because of applied scenarios. The chi-square test was widely used to detect the fault of the state estimates of the filter [10] and of the chi-squared pseu-

dorange residual-based RAIM at measurement level [11]. In this paper, we firstly use the chi-square test for detect fault of carrier observation residual in the position domain.

However, the SSE is a scalar. It does not have redundancy, which is necessary for fault exclusion. We need to extract the fault baseline resolution from all resolutions. In this paper, the baseline multi-frequency solution separation is used for fault exclusion. The solution separation method is a widely implemented method for fault detection [12], [13]. It uses separations of all in view satellites position solution and the solution of satellite subset where the hypothetical fault satellites are removed. In order to use the modified solution separation method for fault exclusion, we develop new separations of hypothetical fault frequency baseline and the all frequency baseline. The separations follow the Gaussian distribution. And the mean of the separations are related to frequency fault, whereas the variances are not. Thus, the maximum likelihood estimation can be used to identify the most likely fault baseline. If there are two or more fault baselines, a grouping method will be used for multi-fault exclusion.

The proposed method fully utilizes the redundancy of the multi-frequency multi-system to solve the multi-value problem, which enhances the robustness and accuracy of the differential positioning. This autonomous fault detection and exclusion method is advantageous in that it can detect and exclude the anomaly of the multi-frequency multi-system positioning system's baseline resolutions effectively; there is no need to account for the correlation between constellations or frequencies; it detects fault in position domain can avoid the effect of the resolution problem in some frequencies; specification of alternative hypotheses for particular applications is unnecessary.

First, the basic model of the high-precision carrier phase differential positioning is discussed. This model is used to resolve the baselines of different frequencies in different navigation systems. Next, an autonomous fault detection and exclusion method for multi-frequency multi-system differential positioning is introduced. A chi-square test is used for fault detection based on carrier observation residual in the position domain. And a new baseline multi-frequency solution separation is used for failure exclusion. The accurate resolutions are effectively fused after detecting and excluding the abnormal baseline resolutions, which could improve the robustness of the system. Then, practical experiments are conducted to validate the performance of the proposed method. Finally, a summary and discussion are presented.

II. HIGH-PRECISION DIFFERENTIAL POSITIONING

In this paper, the used positioning model is based on the orthogonal transformation algorithm suitable for short baseline relative positioning proposed by Chang [14], [15]. The positioning model differs from the common double-differenced model in that it uses Householder transformation to reduce the clock error. This method does not consider the cross-correlation between observations, and the double-differenced integer ambiguity can still be obtained.

The high-precision differential positioning scheme is shown in Fig.1.

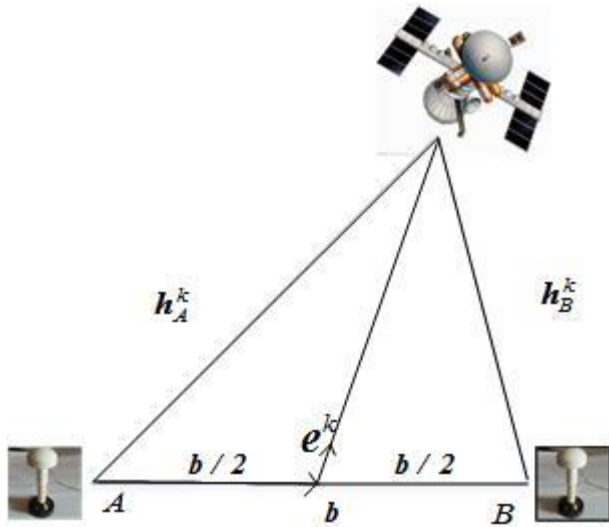A is the base station, and its position is obtained by long-term measurement. The rover is denoted by B. Then suppose

IEEE *Access*

X. Liang *et al.*: GNSS Multi-Frequency Multi-System Highly Robust Differential Positioning Based on an Autonomous FDE Method

FIGURE 1. Geometry of high-precision differential positioning.

that there are m_i visible satellites in frequency L_i (subscript i defines different frequency); we have that

$$\mathbf{y}_{i,S}^{\phi} = \frac{1}{\lambda_i}\mathbf{E}^i \cdot \mathbf{b} - \mathbf{N}_{i,S} + \mathbf{e}\beta + \mathbf{v}_{i,S}^{\phi}, \quad \mathbf{v}_{i,S}^{\phi} \sim N(0, 2\sigma_{\phi,i}^2 I_{m_i})$$
(1)

where:

$\mathbf{y}_{i,S}^{\phi}$ is fractional single-difference phase observations in units of cycles;

$\mathbf{E}^i$ is the $m_i \times 3$ matrix of normalized single-difference line-of-sight vectors;

$\mathbf{v}_{i,S}^{\phi}$ is single-difference phase noise;

$\mathbf{N}_{i,S}$ is the single-difference integer ambiguity vector;

λ_i is the wave length;

$\mathbf{e}$ is a vector of order m_i for which each entry is 1;

β is the clock bias.

Let $\mathbf{P}^i \in R^{m_i \times m_i}$ be a Householder transformation such that

$$\mathbf{P}^i \mathbf{e}_{m_i} = \sqrt{m_i}\mathbf{e}_1, \quad \mathbf{P}^i = \mathbf{I}_{m_i} - \frac{2\mathbf{u}\mathbf{u}^T}{\mathbf{u}^T\mathbf{u}}, \quad \mathbf{u} \equiv \mathbf{e}_1 - \frac{1}{\sqrt{m_i}}\mathbf{e}_{m_i}$$
(2)

with $\mathbf{e}_1 = (1, 0, \cdots, 0)^T = \begin{pmatrix} 1 & \mathbf{0} \end{pmatrix}^T$. Then,

$$\mathbf{P}^i = \left[\begin{array}{c|c} \frac{1}{\sqrt{m_i}} & \frac{\bar{\mathbf{e}}_{m_i-1}^T}{\sqrt{m_i}} \\ \hline \frac{\bar{\mathbf{e}}_{m_i-1}}{\sqrt{m_i}} & \mathbf{I}_{m_i-1} - \frac{\bar{\mathbf{e}}_{m_i-1} \cdot \bar{\mathbf{e}}_{m_i-1}^T}{m_i - \sqrt{m_i}} \end{array} \right] \equiv \left[\begin{array}{c} \mathbf{p}_1^i \\ \bar{\mathbf{P}}^i \end{array} \right]$$
(3)

where $\bar{\mathbf{P}}^i = \left[\frac{\bar{\mathbf{e}}_{m_i-1}}{\sqrt{m_i}} \quad \mathbf{I}_{m_i-1} - \frac{\bar{\mathbf{e}}_{m_i-1}\cdot\bar{\mathbf{e}}_{m_i-1}^T}{m_i-\sqrt{m_i}} \right]$, $\bar{\mathbf{e}}_{m_i-1} = (1, 1, \cdots, 1)^T$. Multiplying (1) by $\mathbf{P}^i$ from the left, we obtain

$$\left[\begin{array}{c} \mathbf{p}_1^i \mathbf{y}_i^{\phi} \\ \bar{\mathbf{P}}^i \mathbf{y}_i^{\phi} \end{array} \right] = \frac{1}{\lambda_i} \left[\begin{array}{c} \mathbf{p}_1^i \mathbf{E}^i \\ \bar{\mathbf{P}}^i \mathbf{E}^i \end{array} \right] \mathbf{b} - \left[\begin{array}{c} \mathbf{p}_1^i \mathbf{N}_{i,S} \\ \bar{\mathbf{P}}^i \mathbf{N}_{i,S} \end{array} \right]$$
$$+ \left[\begin{array}{c} 1 \\ \mathbf{0} \end{array} \right] \sqrt{m_i}\beta + \left[\begin{array}{c} \mathbf{p}_1^i \mathbf{v}_{i,S}^{\phi} \\ \bar{\mathbf{P}}^i \mathbf{v}_{i,S}^{\phi} \end{array} \right]$$
(4)

After the Householder transformation, there are $m_i - 1$ equations that do not include receive clock error β. Thus, we choose the $m_i - 1$ equations, and then,

$$\bar{\mathbf{P}}^i \mathbf{y}_i^{\phi} = \frac{1}{\lambda_i}\bar{\mathbf{P}}^i \mathbf{E}^i \mathbf{b} - \bar{\mathbf{P}}^i \mathbf{N}_{i,S} + \bar{\mathbf{P}}^i \mathbf{v}_{i,S}^{\phi}$$
(5)

Because the Householder transformation is an orthogonal transformation, it does not change the statistical properties of the noise:

$$\bar{\mathbf{P}}^i \mathbf{v}_{i,S}^{\phi} \sim N\left(0, 2\sigma_{i,\varphi}^2 I_{m_i-1}\right)$$
(6)

We introduce the double difference integer ambiguity: $\mathbf{N}_{i,D} = \begin{bmatrix} \mathbf{N}_{2i,S} - \mathbf{N}_{1i,S}, \mathbf{N}_{3i,S} - \mathbf{N}_{1i,S}, \ldots, \mathbf{N}_{mi,S} - \mathbf{N}_{1i,S} \end{bmatrix}^T$. Define $\mathbf{F}^i \equiv \mathbf{I}_{m_i-1} - \frac{\bar{\mathbf{e}}_{m_i-1}\bar{\mathbf{e}}_{m_i-1}^T}{m_i-\sqrt{m_i}}$, $\mathbf{J}^i \equiv \begin{bmatrix} -\bar{\mathbf{e}}_{m_i-1} & \mathbf{I}_{m_i-1} \end{bmatrix}$, we then obtain the equation below:

$$\bar{\mathbf{P}}^i \mathbf{N}_{i,s} = \mathbf{F}^i \mathbf{J}^i \mathbf{N}_{i,s} = \mathbf{F}^i \mathbf{N}_{i,D}$$
(7)

Then, (5) can be rewritten as

$$\bar{\mathbf{P}}^i \mathbf{y}_i^{\phi} = \frac{1}{\lambda_i}\bar{\mathbf{P}}^i \mathbf{E}^i \mathbf{b} - \mathbf{F}^i \mathbf{N}_{i,D} + \bar{\mathbf{P}}^i \mathbf{v}_{i,S}^{\phi},$$
$$\bar{\mathbf{P}}^i \mathbf{v}_{i,S}^{\phi} \sim N\left(0, 2\sigma_{i,\varphi}^2 I_{m_i-1}\right)$$
(8)

Using the orthogonal transformation, we can obtain the double difference integer ambiguity from single difference carrier equations, and the transformed measurements are still uncorrelated.

We define vector $\mathbf{z} = -\mathbf{N}_{i,D}$, which represents the double difference integer ambiguity. Equation (8) becomes

$$\bar{\mathbf{P}}^i \mathbf{y}_i^{\phi} = \frac{1}{\lambda_i}\bar{\mathbf{P}}^i \mathbf{E}^i \mathbf{b} + \mathbf{F}^i \mathbf{z} + \bar{\mathbf{P}}^i \mathbf{v}_{i,S}^{\phi},$$
$$\bar{\mathbf{P}}^i \mathbf{v}_{i,S}^{\phi} \sim N\left(0, 2\sigma_{i,\varphi}^2 I_{m_i-1}\right)$$
(9)

Then, we compute the QR factorization of $\frac{1}{\lambda_i}\bar{\mathbf{P}}^i \mathbf{E}^i$:

$$\mathbf{Q}^T \left(\frac{1}{\lambda_i}\bar{\mathbf{P}}^i \mathbf{E}^i \right) = \left[\begin{array}{c} \mathbf{R} \\ \mathbf{0} \end{array} \right], \quad \mathbf{Q}^T = \left[\begin{array}{c} \mathbf{U} \\ \mathbf{V} \end{array} \right]$$
(10)

where $\mathbf{R}$ is a 3×3 nonsingular upper triangular matrix and $\mathbf{Q}$ is an $(m_i - 1) \times (m_i - 1)$ orthogonal matrix.

Multiplying (9) by $\mathbf{Q}$ from the left yields

$$\left[\begin{array}{c} \mathbf{U}\bar{\mathbf{P}}^i \mathbf{y}_i^{\phi} \\ \mathbf{V}\bar{\mathbf{P}}^i \mathbf{y}_i^{\phi} \end{array} \right] = \left[\begin{array}{c} \mathbf{R} \\ \mathbf{0} \end{array} \right]\mathbf{b} + \left[\begin{array}{c} \mathbf{U}\mathbf{F}^i\mathbf{z} \\ \mathbf{V}\mathbf{F}^i\mathbf{z} \end{array} \right] + \left[\begin{array}{c} \mathbf{U}\bar{\mathbf{P}}^i \mathbf{v}_{i,S}^{\phi} \\ \mathbf{V}\bar{\mathbf{P}}^i \mathbf{v}_{i,S}^{\phi} \end{array} \right]$$
(11)

We eliminate the baseline vector $\mathbf{b}$, obtaining

$$\mathbf{V}\bar{\mathbf{P}}^i \mathbf{y}_i^{\phi} = \mathbf{V}\mathbf{F}^i\mathbf{z} + \mathbf{V}\bar{\mathbf{P}}^i \mathbf{v}_{i,S}^{\phi}, \quad \mathbf{V}\bar{\mathbf{P}}^i \mathbf{v}_{i,S}^{\phi} \sim N\left(0, 2\sigma_{i,\varphi}^2 I_{m_i-4}\right)$$
(12)

Because $\bar{\mathbf{P}}^i$ is $(m_i - 1) \times m_i$, it does not have full column rank, and we will not be able to obtain a unique estimate of $\mathbf{z}$. Thus, we use multi-epoch equations to calculate the float resolution of the double difference integer ambiguity.

The multi-epoch method uses the measurements of many epochs, which increases the data redundancy and model strength considerably. In this manner, a recursive QR decomposition method is used to obtain the float solution of integer ambiguity at the initial time [14]. This approach using the data

X. Liang *et al.*: GNSS Multi-Frequency Multi-System Highly Robust Differential Positioning Based on an Autonomous FDE Method

IEEE *Access*

of two successive epochs can help improve the precision of the float integer ambiguity resolution and avoid large-scale computation, guaranteeing accurate positioning results and numerical stability. The LAMBDA method is then used to fix the integer ambiguity [16].

III. CHI-SQUARE TEST FOR FAULT DETECTION

Because different constellations and different frequencies of the same constellation are independent of each other, each frequency may have positioning resolution biases caused by multipath, problems regarding the hardware devices or other reasons. The fault must be effectively detected after solving the baseline vector separately, avoiding the combination of wrong positioning results.

From (11) we can obtain

$$\mathbf{U}\bar{\mathbf{P}}^i \mathbf{y}_i^\phi = \mathbf{R}\mathbf{b} + \mathbf{U}\mathbf{F}^i \mathbf{z} + \mathbf{U}\bar{\mathbf{P}}^i \mathbf{v}_{i,S}^\phi,$$

$$\mathbf{U}^i \bar{\mathbf{P}}^i \mathbf{v}_{i,S}^\phi \sim N\left(0, 2\sigma_{i,\varphi}^2 I_3\right) \quad (13)$$

When the integer ambiguity $\mathbf{z}$ is obtained, we can obtain

$$\mathbf{U}\bar{\mathbf{P}}^i \mathbf{y}_i^f - \mathbf{U}\mathbf{F}^i \mathbf{z} = \mathbf{R}\mathbf{b} + \mathbf{U}\bar{\mathbf{P}}^i \mathbf{v}_{i,S}^f, \quad \mathbf{U}^i \bar{\mathbf{P}}^i \mathbf{v}_{i,S}^f \sim N\left(0, 2\sigma_{i,\varphi}^2 I_3\right) \quad (14)$$

Defining $\mathbf{P}_0 = \mathbf{U}\bar{\mathbf{P}}^i \mathbf{y}_i^\phi - \mathbf{U}\mathbf{F}^i \mathbf{z}$, $\mathbf{w}_0 = \mathbf{U}^i \bar{\mathbf{P}}^i \mathbf{v}_{i,S}^\phi$ and considering the fault $\mathbf{a}_0$ in the positioning results of the different frequencies, we obtain

$$\mathbf{P}_0 = \mathbf{R}_0 \mathbf{b}_0 + \mathbf{a}_0 + \mathbf{w}_0 \quad (15)$$

By combining multi-frequency together to detect the resolution biases of frequencies, we obtain

$$\mathbf{P}_0 = \begin{bmatrix} \mathbf{P}_{01} \\ \mathbf{P}_{02} \\ \cdots \\ \mathbf{P}_{0n} \end{bmatrix}, \quad \mathbf{R}_0 = \begin{bmatrix} \mathbf{R}_{01} \\ \mathbf{R}_{02} \\ \cdots \\ \mathbf{R}_{0n} \end{bmatrix}, \quad \mathbf{w}_0 = \begin{bmatrix} \mathbf{w}_{01} \\ \mathbf{w}_{02} \\ \cdots \\ \mathbf{w}_{0n} \end{bmatrix},$$

$$\mathbf{a}_0 = \begin{bmatrix} \mathbf{a}_{01} \\ \mathbf{a}_{02} \\ \cdots \\ \mathbf{a}_{0n} \end{bmatrix}, \quad (n \geq 2) \quad (16)$$

where $\mathbf{P}_0$ is a $3n \times 1$ matrix, $\mathbf{R}_0$ is a $3n \times 3$ matrix, and $\mathbf{b}_0$ is a 3×1 matrix. And consistency test requires at least two frequencies' resolutions to be compared for fault detection.

This yields

$$\mathbf{P}_{0n} = \mathbf{R}_{0n} \begin{bmatrix} b_N \\ b_E \\ b_U \end{bmatrix} + \begin{bmatrix} a_{0n_N} \\ a_{0n_E} \\ a_{0n_U} \end{bmatrix} + \mathbf{w}_{0n} \quad (17)$$

Assuming that when a frequency has faults, its fault deviation is defined as $a_{0n_N} = a_{0n_E} = a_{0n_U} = a_i$, and the standard deviation of each frequency in all three baseline directions is σ_i, and the normalization of (15) defines the weight matrix:

$$\mathbf{W}_0 = \begin{bmatrix} \sigma_1^2 & 0 & 0 & 0 & \cdots & 0 & 0 & 0 \\ 0 & \sigma_1^2 & 0 & 0 & \cdots & 0 & 0 & 0 \\ 0 & 0 & \sigma_1^2 & 0 & \cdots & 0 & 0 & 0 \\ 0 & 0 & 0 & \ddots & 0 & 0 & 0 \\ 0 & 0 & 0 & \cdots & 0 & \sigma_n^2 & 0 & 0 \\ 0 & 0 & 0 & \cdots & 0 & 0 & \sigma_n^2 & 0 \\ 0 & 0 & 0 & \cdots & 0 & 0 & 0 & \sigma_n^2 \end{bmatrix}^{-1},$$

$$\mathbf{W}_{0n} = \begin{bmatrix} \sigma_n^2 & 0 & 0 \\ 0 & \sigma_n^2 & 0 \\ 0 & 0 & \sigma_n^2 \end{bmatrix}^{-1} \quad (18)$$

Then, we can obtain

$$\mathbf{W}_0^{1/2} \cdot \mathbf{P}_0 = \mathbf{W}_0^{1/2} \cdot \mathbf{R}_0 \mathbf{b}_0 \mathbf{W}_0^{1/2} \cdot \mathbf{a}_0 + \mathbf{W}_0^{1/2} \cdot \mathbf{w}_0 \quad (19)$$

Defining $\mathbf{P} = \mathbf{W}_0^{1/2} \cdot \mathbf{P}_0, \mathbf{R} = \mathbf{W}_0^{1/2} \cdot \mathbf{R}_0, \mathbf{w} = \mathbf{W}_0^{1/2} \cdot \mathbf{w}_0, \mathbf{a} = \mathbf{W}_0^{1/2} \cdot \mathbf{a}_0$, the equation (19) becomes:

$$\mathbf{P} = \mathbf{R}\mathbf{b}_0 + \mathbf{a} + \mathbf{w} \quad (20)$$

where the elements of $\mathbf{w}$ are independently Gaussian distributed due to the baseline observations are influenced by the multiple sources of errors and the errors between the different frequencies are independent of each other. The left null space of $\mathbf{R}$ is defined as the parity space and denoted as $\mathbf{U}_2$, i.e.,

$$\mathbf{U}_2 \mathbf{R} = 0 \text{ and } \mathbf{U}_2 \mathbf{U}_2^T = \mathbf{I}. \quad (21)$$

The parity vector is defined as:

$$\mathbf{p} = \mathbf{U}_2^T \mathbf{P} \quad (22)$$

Substituting equation (20) and (21) into (22), we have:

$$\mathbf{p} = \mathbf{U}_2(\mathbf{a} + \mathbf{w}) \quad (23)$$

The covariance of $\mathbf{p}$ is obtained as:

$$cov(\mathbf{p}, \mathbf{p}) = \mathbf{U}_2 cov(\mathbf{w}, \mathbf{w})\mathbf{U}_2^T = \mathbf{I} \quad (24)$$

Accordingly, in context of no fault, i.e. $\mathbf{a} = \mathbf{0}$, the parity vector is in the following distribution:

$$\mathbf{p} \sim N(0, \mathbf{I}_{3n-3}) \quad (25)$$

then $\mathbf{p}^T \mathbf{p}$ subjects to chi-square distribution with freedom of $3n - 3$, i.e., $\mathbf{p}^T \mathbf{p} \sim \chi^2(3n - 3)$.

A test statistic is defined as $D_{parity} = \mathbf{p}^T \mathbf{p}$ to perform the following hypothetical test:

$$H_0 : \text{ no fault happens, i.e., } \mathbf{a} = \mathbf{0};$$
$$H_1 : \text{ fault happens, i.e., } \mathbf{a} \neq \mathbf{0}.$$

The hypothesis H_0 is accepted when $D_{parity} \leq T_{\chi^2}$, where the T_{χ^2} is a threshold for fault detection determined by the false alarm probability p_{FA}, i.e., $T_{chi^2} = \chi_{3n-3}^{-2}(p_{FA})$. Otherwise, the hypothesis H_1 is accepted and a fault is detected.

IV. BASELINE MULTI-FREQUENCY SOLUTION SEPARATION FOR FAILURE EXCLUSION

After the fault detection, in order to avoid the fusion of fault baselines, a fault baseline exclusion process is required. In (20), because there should be at least three frequencies, $n \geq 3$ must be satisfied to achieve the fault exclusion of redundancy requirements.

We assume that $\hat{\mathbf{b}}_{00}$ is the maximum probability estimation of the baseline vector under the no-fault assumption. The estimated values of (15) and (17) for the baseline vector are obtained using the least-squares method.

$$\hat{\mathbf{b}}_0 = (\mathbf{R}_0^T \mathbf{W}_0 \mathbf{R}_0)^{-1} \mathbf{R}_0^T \mathbf{W}_0 \mathbf{P}_0 \quad (26)$$

$$\hat{\mathbf{b}}_{0n} = (\mathbf{R}_{0n}^T \mathbf{W}_{0n} \mathbf{R}_{0n})^{-1} \mathbf{R}_{0n}^T \mathbf{W}_{0n} \mathbf{P}_{0n} \quad (27)$$

IEEE *Access*

X. Liang *et al.*: GNSS Multi-Frequency Multi-System Highly Robust Differential Positioning Based on an Autonomous FDE Method

Define test statistic vectors as $\mathbf{q}_0 = \hat{\mathbf{b}}_0 - \hat{\mathbf{b}}_{00}$ and $\mathbf{q}_{0n} = \hat{\mathbf{b}}_{0n} - \hat{\mathbf{b}}_{00}$. As seen from the above mathematical model, the following hypothesis test is

$$H_0 : E\{\mathbf{q}_i\} = \mathbf{0}; D\{\mathbf{q}_i\} = \delta_i^2, (i = 0, 01, 02\ldots 0n) \left.\right\}$$
$$H_1 : E\{\mathbf{q}_i\} = \boldsymbol{\mu}_i; D\{\mathbf{q}_i\} = \delta_i^2, (i = 0, 01, 02\ldots 0n) \left.\right\}$$
(28)

where $\boldsymbol{\mu}_i = E\{\mathbf{q}_i\} = (\mathbf{R}_i^T \mathbf{W}_i \mathbf{R}_i)^{-1} \mathbf{R}_i^T \mathbf{W}_i \mathbf{a}_i$ and $\delta_i^2 = (\mathbf{R}_i^T \mathbf{W}_i \mathbf{R}_i)^{-1}$.

Constructing a new test statistic vector $\mathbf{g}_i = \hat{\mathbf{b}}_{0i} - \hat{\mathbf{b}}_0$, $(i = 1, 2\ldots n)$, the following hypothesis test exists:

$$H_0' : E\{\mathbf{g}_i\} = \mathbf{0}; D\{\mathbf{g}_i\} = \delta_{0i}^2 - \delta_0^2, (i = 1, 2\ldots n) \left.\right\}$$
$$H_1' : E\{\mathbf{g}_i\} = \boldsymbol{\mu}_{0i} - \boldsymbol{\mu}_0; D\{\mathbf{g}_i\} = \delta_{0i}^2 - \delta_0^2, (i = 1, 2\ldots n) \left.\right\}$$
(29)

Because the three baseline directions of the NEU coordinate component are related, the three direction vectors of the frequency baseline resolution must be separated. After identifying a fault in one direction, the frequency resolution must be faulted. We choose the test statistic of the north direction vector to identify the faults. Its probability density function is

$$p(g_i) = \frac{1}{[2\pi(\delta_{0i}^2 - \delta_0^2)]^{1/2}} \exp\left\{-\frac{[g_i - (\mu_{0i} - \mu_0)]^2}{2(\delta_{0i}^2 - \delta_0^2)}\right\}$$
(30)

In the multi-frequency system, the following processes are different for single-fault and multi-fault, we discuss them respectively.

(1) Assuming that only one frequency has faults at a time:

$$\mathbf{a}_0 = \begin{bmatrix} 0 & \cdots & a_{0i_N}, a_{0i_E}, a_{0i_U} & \cdots & 0 \end{bmatrix}^T$$
$$= a_i \begin{bmatrix} 0 & \cdots & 1, 1, 1 & \cdots & 0 \end{bmatrix}^T$$
(31)

Because the value of a_i is unknown, the maximum likelihood estimation method is used to estimate its value. According to the concept of maximum likelihood estimation, when the maximum likelihood estimate value of a_i is reached, the probability density function $p(g_i)$ is $-\frac{1}{2}[g_i - (\mu_{0i} - \mu_0)]^2$, which is maximized as well. The derivation is as follows:

$$-\frac{1}{2}[g_i - (\mu_{0i} - \mu_0)]^2$$
$$= -\frac{1}{2}\left\{\left[g_i - (\mathbf{R}_i^T \mathbf{W}_i \mathbf{R}_i)^{-1}\mathbf{R}_i^T\mathbf{W}_i\mathbf{a}_i\right.\right.$$
$$\left.\left. -(\mathbf{R}_0^T \mathbf{W}_0 \mathbf{R}_0)^{-1}\mathbf{R}_0^T\mathbf{W}_0\mathbf{a}_0\right]_F\right\}^2$$
$$= -\frac{1}{2}\left\{g_i - a_i\left[(\mathbf{R}_i^T \mathbf{W}_i \mathbf{R}_i)^{-1}\mathbf{R}_i^T\mathbf{W}_i\mathbf{e}\right.\right.$$
$$\left.\left. -(\mathbf{R}_0^T \mathbf{W}_0 \mathbf{R}_0)^{-1}\mathbf{R}_0^T\mathbf{W}_0\mathbf{l}\right]_F\right\}^2$$
$$= a_i g_i \left[(\mathbf{R}_i^T \mathbf{W}_i \mathbf{R}_i)^{-1}\mathbf{R}_i^T\mathbf{W}_i\mathbf{e} - (\mathbf{R}_0^T \mathbf{W}_0 \mathbf{R}_0)^{-1}\mathbf{R}_0^T\mathbf{W}_0\mathbf{l}\right]_F$$
$$- \frac{a_i^2}{2}\left[(\mathbf{R}_i^T \mathbf{W}_i \mathbf{R}_i)^{-1}\mathbf{R}_i^T\mathbf{W}_i\mathbf{e} - (\mathbf{R}_0^T \mathbf{W}_0 \mathbf{R}_0)^{-1}\mathbf{R}_0^T\mathbf{W}_0\mathbf{l}\right]_F^2$$
$$- \frac{g_i^2}{2}$$
(32)

where $\mathbf{l} = [0, 1, 1, 1, 0]^T$ and $[]_F$ represents the first row of the matrix.

Equation (32) takes the derivative of a_i; then, letting the equation equal to zero, the maximum likelihood estimate of the parameter a_i is obtained as $\hat{a}_i$.

This estimate maximizes $-\frac{1}{2}[g_i - (\mu_{0i} - \mu_0)]^2$ and the probability density function

$$p(g_i) = \frac{1}{[2\pi(\delta_{0i}^2 - \delta_0^2)]^{1/2}} \exp\left\{-\frac{[g_i - (\mu_{0i} - \mu_0)]^2}{2(\delta_{0i}^2 - \delta_0^2)}\right\},$$

making it reach the maximum $p(g_i)_{\max}$. The frequency with the highest probability density in all measured frequencies is the most likely fault frequency.

(2) Assuming that two or more frequencies may have faults at a time,

$$\mathbf{a}_0 = \begin{bmatrix} 0 & \cdots & a_{0i_N}, a_{0i_E}, a_{0i_U} & \cdots & a_{0j_N}, a_{0j_E}, a_{0j_U} & \cdots & 0 \end{bmatrix}^T$$
(33)

When two frequencies have faults at the same time, equation (32) becomes

$$-\frac{1}{2}[g_i - (\mu_{0i} - \mu_0)]^2$$
$$= -\frac{1}{2}\left\{g_i - \left[(\mathbf{R}_i^T \mathbf{W}_i \mathbf{R}_i)^{-1}\mathbf{R}_i^T\mathbf{W}_i\mathbf{a}_i\right.\right.$$
$$\left.\left. -(\mathbf{R}_0^T \mathbf{W}_0 \mathbf{R}_0)^{-1}\mathbf{R}_0^T\mathbf{W}_0\mathbf{a}_0\right]_F\right\}^2$$
$$= -\frac{1}{2}\left\{g_i - a_i\left[(\mathbf{R}_i^T \mathbf{W}_i \mathbf{R}_i)^{-1}\mathbf{R}_i^T\mathbf{W}_i\mathbf{e}\right.\right.$$
$$\left.\left. -(\mathbf{R}_0^T \mathbf{W}_0 \mathbf{R}_0)^{-1}\mathbf{R}_0^T\mathbf{W}_0\mathbf{l}'\right]_F\right\}^2 \quad (34)$$

where $\mathbf{l}' = [0, 1, 1, 1, 0, a_j/a_i, a_j/a_i, a_j/a_i, 0]^T$.

Equation (34) consists of two unknowns. If we use the maximum likelihood solution, the maximum likelihood estimate is related to a_j. The two failures cannot be distinguished, and thus, the maximum likelihood estimation is no longer available for multi-fault exclusion.

Thus, the grouping method is used to help exclude the multiple faults. Fig.2 shows the procedure for the grouping method of multi-fault exclusion. First, we suppose that there is only a single fault. The single-fault exclusion method is adopted to exclude the single fault. Then, the detection method is used to detect the remaining frequency baseline resolutions. If the fault can still be detected, the frequencies of the system are considered to have a multi-failure problem. Then, we remove the relevant parameters of different frequencies for testing in turn until the remaining frequency baseline resolutions have no faults detected. In this manner, there is no failure baseline resolution in the remaining frequencies. In particular, when grouping into groups with two frequencies, all groups detect faults after fault detection based on the consistency of the baseline resolutions. This means that only one frequency baseline resolution of all frequencies is not faulty or all frequency baseline resolutions are faulty. Because we cannot effectively determine which situation it is at this time, system failure is defined. We can obtain the current baseline resolution according to the Kalman filter based on the last moment. We set the alarm time threshold for the positioning system, and if the duration of the defined

X. Liang *et al.*: GNSS Multi-Frequency Multi-System Highly Robust Differential Positioning Based on an Autonomous FDE Method

IEEE *Access*

system fault is larger than the alarm threshold, the system will assess the fault of the positioning system and transmit alarm information. For the obtained fault-free baseline resolutions of different frequencies, the weighted values for different frequencies can be determined according to the measurement accuracy of carrier phase. Then, to obtain the optimal baseline solution, the optimally weighted average solution (OWAS) method can be used to combine the baseline resolutions at the same time [17].

$$b = \frac{w_1 b_1 + w_2 b_2 + w_3 b_3 + w_4 b_4 + w_5 b_5}{w_1 + w_2 + w_3 + w_4 + w_5} \quad (35)$$

where $w_1 = 1/\sigma_{1,\varphi}^2, w_2 = 1/\sigma_{2,\varphi}^2, w_3 = 1/\sigma_{3,\varphi}^2,$ $w_4 = 1/\sigma_{4,\varphi}^2, w_5 = 1/\sigma_{5,\varphi}^2.$

V. REAL DATA TESTS

To validate the performance of the autonomous fault detection and exclusion method in GNSS multi-frequency multi-system differential positioning, tests on real data from the Shanmei dam in Quanzhou, Fujian Province, China were conducted using this highly robust system to monitor the deformation of the dam. The test scene is shown in Fig.3.

The antennas used in the monitoring system are HX-BS781A antennas of BDStar Navigation, which support the L1/L2 frequencies of GPS, the B1/B2/B3 frequencies of BD and L1/L2 frequencies of GLONASS, and the low noise amplifier gain is 40 dB. The receivers are Novatel BDM610 GNSS, which offer GPS L1/L2 and BD B1/B2/B3 frequencies and the measurement accuracies of the five frequencies are all 1 mm. The data update frequency is 1 Hz. The computers at the monitoring station, base station and control center are connected to the switch through LAN. At the site of the dam, the baseline length is measured to be 260 m using a commercial system designed by the Huace Company. The measurement time is 78,694 epochs (approximately 22 h). We define the faults, such as multipath, cycle-slip, and visible satellite-deficient faults and integer ambiguity resolution failure, all as software resolution failures to describe the faults more intuitively and visually. Problems involving the network, receivers and other factors, which cause observation measurement failure, are defined as hardware failures.

The method of fault detection and exclusion fixes the integer ambiguities of each frequency but does not need to consider the strong correlation between different constellations or the different frequencies of same constellation. The consistencies of the baseline resolutions at five frequencies are detected using the faulty detection method described above. Because the measurement accuracy $\sigma_{i,\varphi}$ of all five frequencies is 0.001 m, according to (14), we can obtain the weight of the carrier observation equation ($\sigma_i^2 = 2 \times 0.001^2 = 2 \times 10^{-6}$) and bring the weight into the weight matrix for a normalized solution. The maximum probability density function solution obtained using the maximum likelihood method is used to detect single faults, and the grouping method is used to detect multiple faults. When there are only two frequency baseline resolutions in each group and no group meets the requirements of the consistency test, only one frequency baseline resolution of the five frequencies or no frequency baseline resolution is fault-free. At this
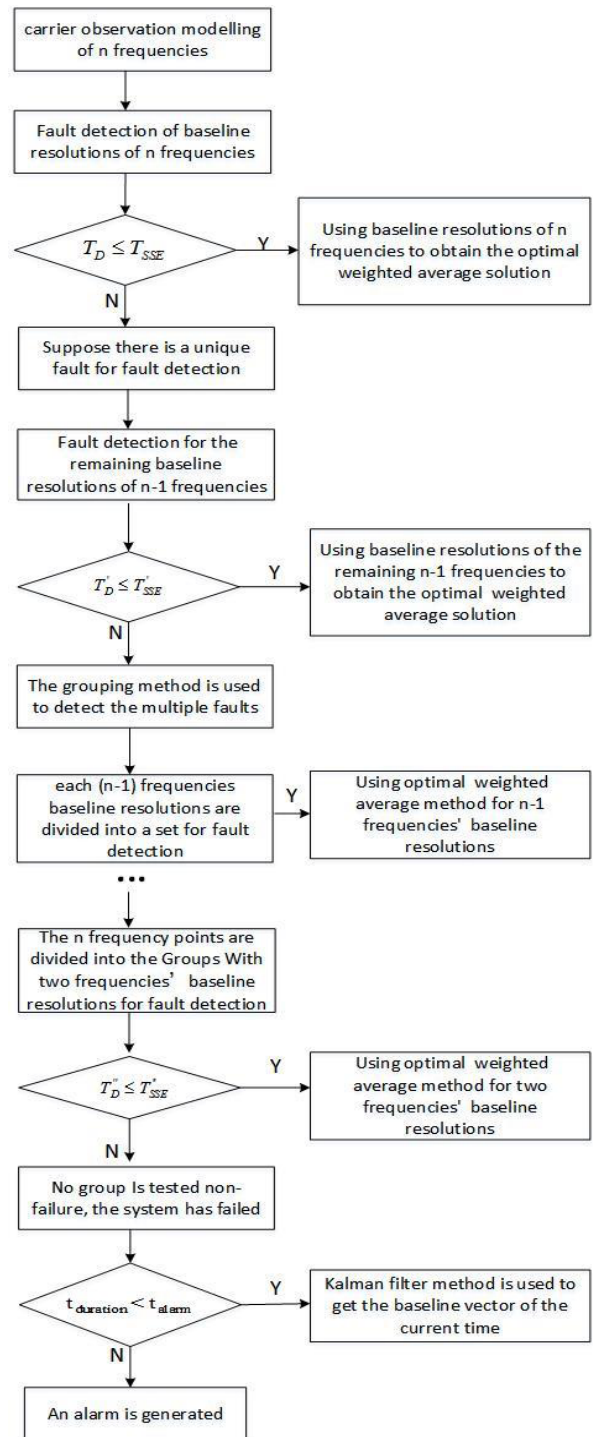

FIGURE 2. Flowchart for the grouping method for multi-fault exclusion.

point, the system can be considered to have a failure, and the Kalman filter method can be used for the baseline resolution, which is not discussed.

Defining the sum of the squares of the components of the carrier observation vector residuals as $F_{SSE} = \mathbf{p}^T \mathbf{p}$, the fault test statistic is:
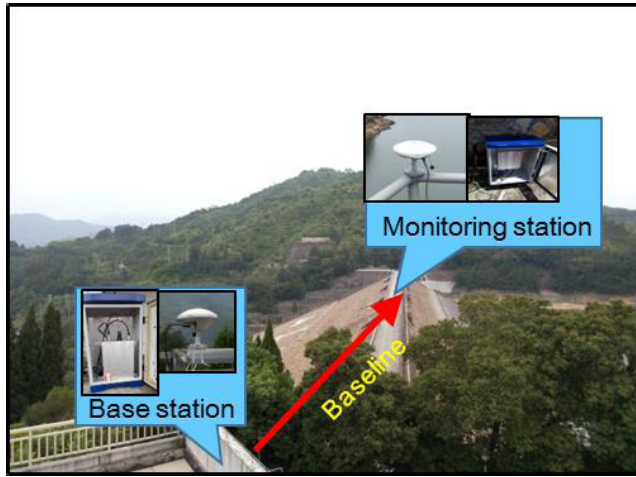
$$T_X = \sqrt{F_{SSE} / (3n - 3)} \quad (36)$$

FIGURE 3. Actual test scene of the Shaimei dam.

FIGURE 4. Distributions of the baseline lengths of the combined five frequencies through the proposed method, and the L1, L2, B1, B2, B3 frequencies for the dam testing.

F_{SSE} follows the chi-square distribution. The cumulative distribution function of chi-squared distribution is expressed as

$$P(x^2; v) = \int_0^{x^2} \frac{1}{2\Gamma(v/2)} (x^2/2)^{v/2-1} e^{-x^2/2} dx^2 \quad (37)$$

where x is the variable, and v denotes the freedom.

The quantity of the probability of false alarm as $P_{fa} = 10^{-5}$ is expressed as:

$$x_i^2 = \chi^{-2}(P_{fa}, v_i) \quad (38)$$

Then, the baseline resolutions of the five frequencies are divided into group of five-frequency baseline resolutions, four-frequency baseline resolutions, three-frequency baseline resolutions, and two-frequency baseline resolutions; the detection thresholds of these groups are shown below:

$$T_d^1 = \sqrt{x_1^2/(3n-3)} = \sqrt{45/(5 \times 3 - 3)} \approx 1.9365 \quad (39)$$

$$T_d^2 = \sqrt{x_2^2/(3n-3)} = \sqrt{40/(4 \times 3 - 3)} \approx 2.1082 \quad (40)$$

$$T_d^3 = \sqrt{x_3^2/(3n-3)} = \sqrt{33/(3 \times 3 - 3)} \approx 2.3452 \quad (41)$$

$$T_d^4 = \sqrt{x_4^2/(3n-3)} = \sqrt{26/(2 \times 3 - 3)} \approx 2.9439 \quad (42)$$

The fault is detected by comparing T_X and T_d: if $T_X < T_d$, there is no fault in the baseline resolutions of the group; if $T_X > T_d$, a fault is considered to exist in the group, in which case fault exclusion is necessary.

The results of the baseline resolution obtained by combining the baseline resolutions of the five frequencies using the proposed fault detection and exclusion method are compared with the results of each frequency baseline resolution. The test results are shown in Figs. 4-7.

The figures illustrate that the results of the single-frequency baseline resolution do not have high robustness, particularly for the BD system. Therefore, it is impossible to accurately monitor the deformation of the dam at present using a single frequency. Instead, multiple frequencies must be used and fault detection and exclusion must be performed
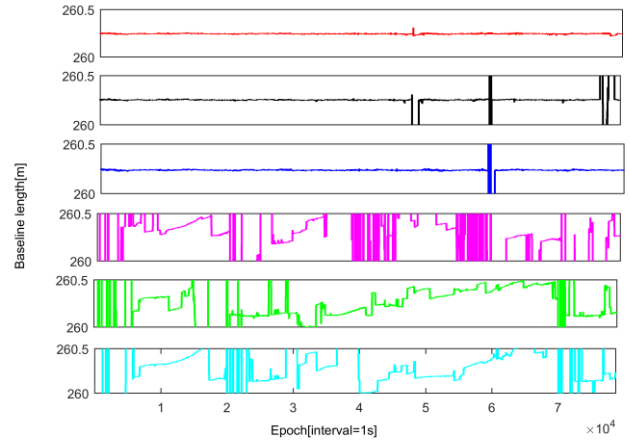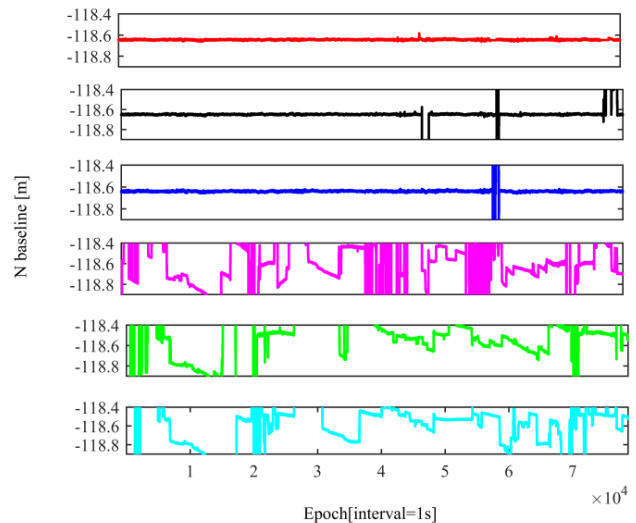

FIGURE 5. Distributions of the N baselines of the combined five frequencies through the proposed method, and the L1, L2, B1, B2, B3 frequencies for the dam testing.
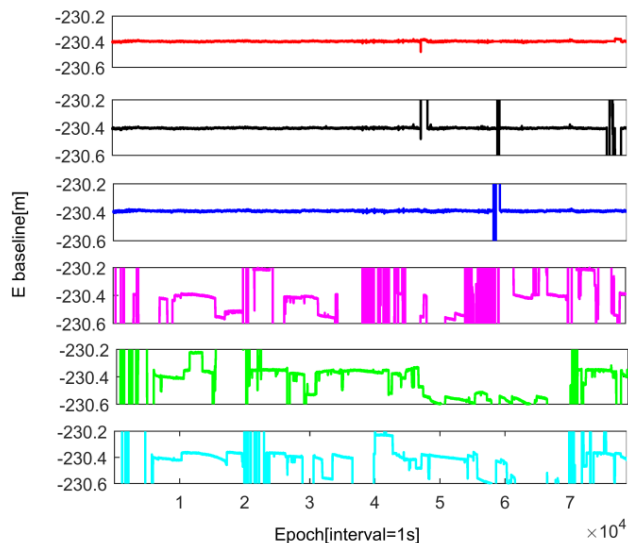
TABLE 1. Baseline resolution results of the dam testing obtained using the autonomous detection and exclusion method.

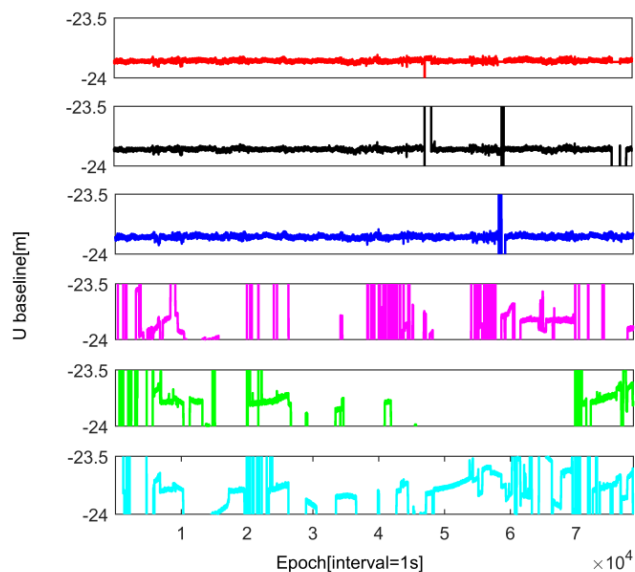| Parameter	Standard deviation (m)	Mean (m)
baseline length	0.004	260.25
N baseline	0.004	-118.64
E baseline	0.004	-230.40
U baseline	0.009	-23.85

to obtain accurate baseline resolution results. The baseline resolution results are shown in Table. 1.

The horizontal accuracy of the monitoring system is below 5 mm, and the vertical accuracy is below 10 mm, which are accordance with the accuracy requirement of the Shanmei dam deformation monitoring. The system ensures the robustness of the baseline resolution using the described method.

Table. 2 illustrates that the baseline resolutions of the L1, B2, and B3 frequencies are consistent in region 1 of Fig.8,

X. Liang *et al.*: GNSS Multi-Frequency Multi-System Highly Robust Differential Positioning Based on an Autonomous FDE Method

IEEE *Access*

FIGURE 6. Distributions of the E baselines of the combined five frequencies through the proposed method, and the L1, L2, B1, B2, B3 frequencies for the dam testing.
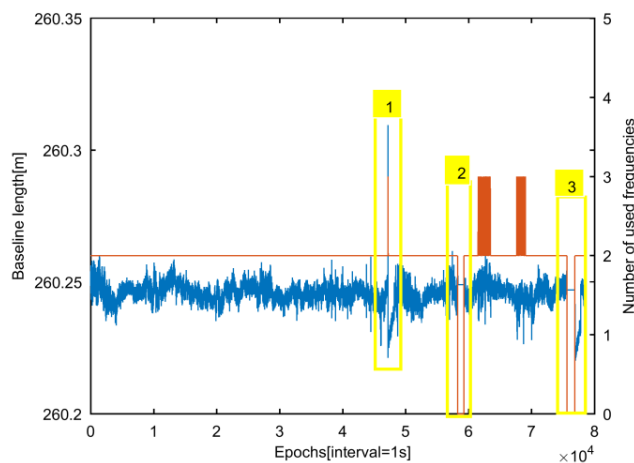

FIGURE 7. Distributions of the U baselines of the combined five frequencies through the proposed method, and the L1, L2, B1, B2, B3 frequencies for the dam testing.

TABLE 2. Analysis results of the abnormal regions.

Parameter	Region 1	Region 2	Region 3
Detection threshold T_d	$T_d^3 = 2.3452$	$T_d^4 = 2.9439$	$T_d^4 = 2.9439$
Fault test statistic T_X	2.3391	40.5334	3.35
Used frequencies	L1/B2/B3	0	0
L1 baseline length (m)	260.31	260.26	260.67
L2 baseline length (m)	260.24	59654.57	260.24
B1 baseline length (m)	260.69	258.93	259.62
B2 baseline length (m)	260.31	260.46	260.12
B3 baseline length (m)	260.31	260.35	260.14
Baseline length of the five frequencies (m)	260.31	260.25	260.25
Duration (s)	1	356	559
Alarm	No	No	Yes

FIGURE 8. Distributions of the baseline length and the corresponding number of frequencies used for the dam monitoring system.

the baseline resolution is recursive repeated from the previous time by the Kalman filter. Because this is an example of a high-precision positioning application for dam deformation monitoring, the timeliness requirement of the dam monitoring is less stringent. Thus, we set the alarm time threshold as 6 min. Because region 3 is unable to achieve multi-frequency multi-system baseline resolution consistency for a relatively long time, the alarm is triggered.

Fig. 9 shows the distributions of the visible satellites for each frequency. The visible satellites are numbered after filtering out the satellites with large cycle-slip through a simple three-difference cycle-slip test method. There are still several small cycle slips of the satellites that cannot be filtered out. Due to the environment in which the dam is located, the BD GEO satellites with a low elevation angle are easily obscured, and the probabilities of frequency occlusions and cycle slips of the three BD frequencies are relatively high, which affects the positioning accuracy. The GPS signal is stable for the majority of the testing time, but both the L1 and L2 frequencies are reinitialized due to a network interruption. The L1 and L2 frequencies are also affected by the cycle slips. Failure may cause short-term integer ambiguity resolutions to be inaccurate, affecting the positioning results. Therefore, due to software resolution and hardware failure the final positioning results are affected.
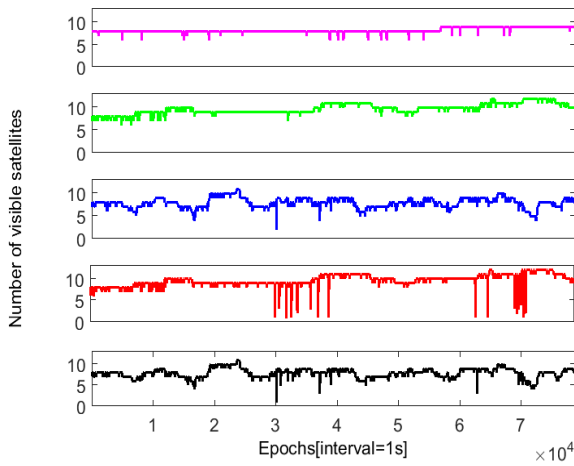
and the detection is adopted without failure. At this point, the missing alarm is triggered. The integration of the fault baseline resolutions leads to an error. Because the three frequencies are independent, the probabilities of simultaneous failure and of the fault baseline resolutions meeting satisfying the consistency requirement are extremely small. At this point, the missing alarm is triggered. The integration of the fault baseline resolutions leads to an error. Regions 2 and 3 are the result of a system failure. Until the baseline resolutions of the two frequencies are grouped, no group meets satisfies the requirement for detection consistency, which results in this situation being defined as system failure. Moreover,

IEEE *Access*

X. Liang *et al.*: GNSS Multi-Frequency Multi-System Highly Robust Differential Positioning Based on an Autonomous FDE Method

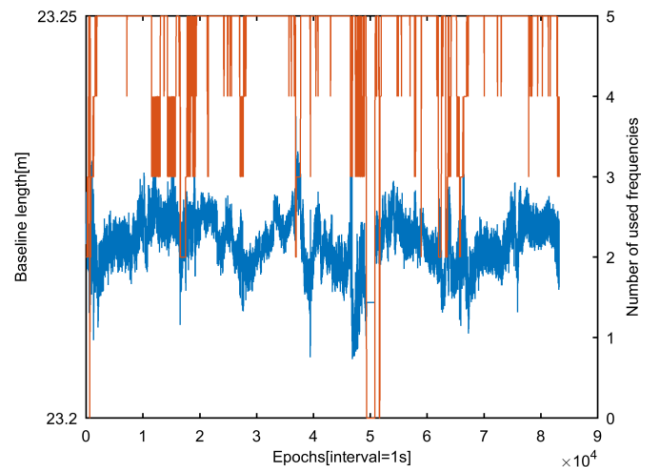**FIGURE 9.** Distributions of the visible satellites at the L1, L2, B1, B2, and B3 frequencies.

FIGURE 11. Distributions of the baseline length and corresponding number of frequencies used for the roof testing.

TABLE 3. Fault statistics of the GPS L1/L2 and BD B1/B2/B3 frequencies.

Frequency	Total cumulative epochs of software resolution faults	Total cumulative epochs of hardware faults	Probability of failure (Epochs of failures/Total testing epochs)
GPS L1	391	1582	2.4%
GPS L2	28	1056	1.3%
BD B1	421	521	1.1%
BD B2	221	2484	3.2%
BD B3	507	1429	2.3%

TABLE 4. Baseline resolution results of the roof testing after using the autonomous detection and exclusion method.

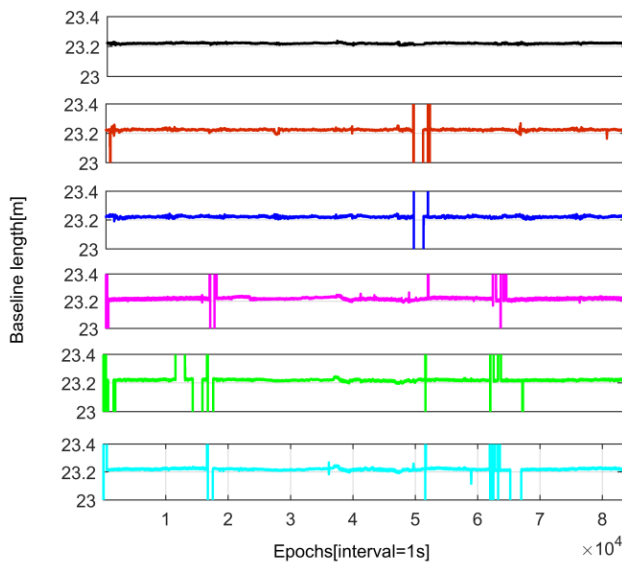| Parameter	Standard deviation (m)	Mean (m)
baseline length	0.003	23.22
N baseline	0.003	-9.73
E baseline	0.002	20.69
U baseline	0.009	4.04

FIGURE 10. Distributions of the baseline lengths of the combined five frequencies through the proposed method, and the L1, L2, B1, B2, B3 frequencies for the roof testing.

Because of the surrounding environment of the dam, the available frequencies are always no more than three; thus, we perform the experiment in an open space on the roof of the New Main Building of Beihang University, Beijing, China.

The hardware used in the experiment is identical to that on the dam. The observation epoch is 83,851 (approximately 23.3 h), and the measured baseline length is approximately 23.2 m. The resulting baseline resolutions for this test are compared in Fig.10.

Fig.11 illustrates that when the five frequencies are all in good condition, the result combines of all five frequencies in the majority of cases. All five frequencies baseline resolutions are used in 81% of the case. The reasons for the failures of each frequency resolution are shown in Table. 3.

Because the probability of failure for each frequency is independent and some failures of different frequencies occur at different times, a direct combination will result in the

failure probability of the positioning solution of the multi-frequency multi-system positioning system is up to 5%. The proposed method can detect and exclude software resolution faults and hardware faults effectively. Via the autonomous fault detection and exclusion, excluding the deviate positioning solutions can effectively avoid the faults in Table. 3, and the final baseline resolution results are shown in Table. 4. Via the autonomous fault detection and exclusion, the faults in Table 3 can effectively be avoided by excluding the frequency deviant position solution; the final baseline resolution result is shown in Table 4.

VI. SUMMARY

We propose an autonomous fault detection and exclusion algorithm. Using the high-accuracy carrier phase differential positioning model to resolve the baselines of different systems and different frequencies, the correlation between the systems and the frequencies can be effectively avoided. Then the chi-square test for fault detection and the modified

X. Liang *et al.*: GNSS Multi-Frequency Multi-System Highly Robust Differential Positioning Based on an Autonomous FDE Method

IEEE *Access*

solution separation for fault exclusion are proposed. These methods can detect and exclude the failure resolutions effectively, regardless of whether the fault baseline resolution of the frequency is caused by a software resolution fault or a hardware fault. The results of experiments show that the proposed method can effectively detect and exclude most of the frequency positioning deviations caused by software resolution faults and hardware faults, and achieves high robustness for the differential positioning system.

REFERENCES

[1] R. Hatch, "The synergism of GPS code and carrier measurements," in *Proc. Int. Geodetic Symp. Satellite Doppler Positioning*, 1983, pp. 1213–1231.

[2] J. M. F. Ordonez *et al.*, "First experiences with differential GLONASS/GPS positioning," in *Proc. ION GPS*, Albuquerque, NM, USA, Sep. 1992, pp. 153–158.

[3] H. He, J. Li, Y. Yang, J. Xu, H. Guo, and A. Wang, "Performance assessment of single- and dual-frequency BeiDou/GPS single-epoch kinematic positioning," *GPS Solutions*, vol. 18, no. 3, pp. 393–403, 2014, doi: 10.1007/s10291-013-0339-3.

[4] F.-Y. Chu and M. Yang, "GPS/Galileo long baseline computation: Method and performance analyses," *GPS Solutions*, vol. 18, no. 2, pp. 263–272, 2014, doi: 10.1007/s10291-013-0327-7.

[5] C. D. de Jong, H. van der Marel, and N. F. Jonkman, "Real-time GPS and GLONASS integrity monitoring and reference station software," *Phys. Chem. Earth A, Solid Earth Geodesy*, vol. 26, nos. 6–8, pp. 545–549, 2001, doi: 10.1016/S1464-1895(01)00098-9.

[6] A. El-Mowafy, "GNSS multi-frequency receiver single-satellite measurement validation method," *GPS Solutions*, vol. 18, no. 4, pp. 553–561, 2014, doi: 10.1007/s10291-013-0352-6.

[7] D. Kim and R. B. Langley, "Instantaneous real-time cycle-slip correction for quality control of GPS carrier-phase measurements," *Navigation*, vol. 49, no. 4, pp. 205–222, 2002, doi: 10.1002/j.2161-4296.2002.tb00269.x.

[8] M. Sahmoudi and R. Landry, "A nonlinear filtering approach for robust multi-GNSS RTK positioning in presence of multipath and ionospheric delays," *IEEE J. Sel. Topics Signal Process.*, vol. 3, no. 5, pp. 764–776, Oct. 2009, doi: 10.1109/JSTSP.2009.2033158.

[9] P. R. R. Strode and P. D. Groves, "GNSS multipath detection using three-frequency signal-to-noise measurements," *GPS Solutions*, vol. 20, no. 3, pp. 399–412, 2016, doi: 10.1007/s10291-015-0449-1.

[10] B. Brumback and M. Srinath, "A Chi-square test for fault-detection in Kalman filters," *IEEE Trans. Autom. Control*, vol. 32, no. 6, pp. 552–554, Jun. 1987.

[11] M. Joerger and B. Pervan, "Fault detection and exclusion using solution separation and chi-squared ARAIM," *IEEE Trans. Aerosp. Electron. Syst.*, vol. 52, no. 2, pp. 726–742, Apr. 2016.

[12] X.-W. Chang, C. C. Paige, and C. C. J. M. Tiberius, "Computation of a test statistic in data quality control," *SIAM J. Sci. Comput.*, vol. 26, no. 6, pp. 1916–1931, 2005.

[13] J. Blanch, T. Walter, and P. Enge, "RAIM with optimal integrity and continuity allocations under multiple failures," *IEEE Trans. Aerosp. Electron. Syst.*, vol. 46, no. 3, pp. 1235–1247, Jul. 2010, doi: 10.1109/TAES.2010.5545186.

[14] X.-W. Chang and C. C. Paige, "An orthogonal transformation algorithm for GPS positioning," *SIAM J. Sci. Comput.*, vol. 24, no. 5, pp. 1710–1732, 2003, doi: 10.1137/S1064827501397937.

[15] X.-W. Chang, C. C. Paige, and L. Yin, "Code and carrier phase based short baseline GPS positioning: Computational aspects," *GPS Solutions*, vol. 9, no. 1, pp. 72–83, 2005, doi: 10.1007/s10291-004-0112-8.

[16] P. J. G. Teunissen, "The least-squares ambiguity decorrelation adjustment: A method for fast GPS integer ambiguity estimation," *J. Geodesy*, vol. 70, no. 1, pp. 65–82, 1995.

[17] Y. C. Lee, "A new improved RAIM method based on the optimally weighted average solution (OWAS) under the assumption of a single fault," in *Proc. ION NTM Inst. Navigat.*, Monterey, CA, USA, Jan. 2006, pp. 574–586.

XIAO LIANG was born in Zhengzhou, China, in 1991. She received the B.S. degree in electrical engineering from Zhengzhou University, China, in 2013. She is currently pursuing the Ph.D. degree with the School of Electronic and Information Engineering, Beihang University. Her research interests focus on GNSS differential positioning and attitude determination.

ZHIGANG HUANG received the Ph.D. degree from Beihang University in 2004. He is currently a Professor with the School of Electronics and Information Engineering, Beihang University. His research interests include GNSS differential algorithms and satellite navigation.

HONGLEI QIN received the B.S. degree in computer application from the Changchun Institute of Technology, China, in 1996, and the M.S. degree in electrical engineering from the Harbin Institute of Technology, China, and the Ph.D. degree in navigation guided and control from the Harbin Engineering University, China, in 2001. He is currently a Professor with Beihang University. His research interests are automatic test system and fault diagnosis, and satellite navigation

YICHEN LIU received the B.E. degree in electronic science and technology from Xidian University, China, in 2015. He is currently pursuing the master's degree with the School of Electronic and Information Engineering, Beihang University. His research interests focus on GNSS high precision dynamic positioning.

• • •